Light Scattering from Two-Dimensional Periodic Arrays of Noble-Metal Disks and Complementary Circular Apertures

Xiaowei Ji[1], Daiki Sakomura[1], Akira Matsushima[1, *], and Taikei Suyama[2]

Abstract—Numerical solution is presented for light scattering from two kinds of free-standing periodic arrays, that is, disks made of noble-metal and circular apertures perforated in a thin noble-metal sheet. The shapes of them are complementary to each other, and the circular areas are allocated along two orthogonal coordinates with the same periodicity. Using the generalized boundary conditions of the surface impedance type, we formulate the boundary value problem into a set of integral equations for unknown electric and magnetic current densities defined over the circular area. Employment of the method of moments allows us to solve the integral equations and give the expansion coefficients of the current densities, from which we can find reflected, transmitted, and absorbed powers. Dependence of the powers on the array parameters and wavelength is discussed in detail from the viewpoint of grating resonance. Special attention is paid to the extraordinary transmission which occurs in the arrays of apertures of sub-wavelength size by analytical derivation of the quasi-static solutions.

1. INTRODUCTION

With growing interests in recent technology of controlling lightwaves, it has become necessary to accurately evaluate the optical properties of surface plasmon polaritons [1, 2]. One effective means of facilitating plasmon resonances and enhancing near electromagnetic field is to put multiple nano-metallic particles close to each other or to compile them into periodic structures. For infinitely long noble-metal scatterers having one-dimensional periodicity, fruitful results have been reported upon circular cylinders [3] and flat strips [4, 5], in which the observed resonances are analytically classified into the local and mutual (due to periodicity) types. These considerations are so instructive that the extension of the conception into two-dimensional geometries related with spheres or disks would be worth a lot. It is known that one of such structures, that is, a metallic plate periodically perforated with cylindrical holes, exhibits so called the extraordinary optical transmission [6, 7] even though the size of aperture cross section is in the order of sub-wavelength. This originates from excitation of surface waves on both sides of the plate. Then analytical approach to understanding its mechanism becomes also an interesting subject.

In view of the above background, the present paper deals with free-standing arrays of disks and apertures as fundamental periodic plane structures. The problem of plane wave scattering is formulated by applying the generalized boundary conditions [8] which replace the effect of electric constants and thickness of the nano-metal with both electric resistance and magnetic conductance if the metal thickness is much smaller than the wavelength. Contrary to the use of only one type of surface impedance [9], the incorporation of these two constants is essential in coping with long and short range surface plasmons (LRSP and SRSP), and therefore this set of conditions has successively been applied to the strip problems [4, 5, 10]. The electromagnetic field is expanded by Floquet modes, which were frequently

employed in the analysis of frequency selective surfaces [11] and waveguide phased arrays [12] in the microwave region. Combination of the above conditions and expansions leads us to a set of integral equations for unknown electric and magnetic current densities defined on the circular area. Using the method of moments, we obtain the numerical solution of the integral equations and give the expansion coefficients of the current densities, from which we can find power distributions. The behavior of the transmitted, reflected, and absorbed powers are examined in detail from the viewpoint of resonances. We try to reveal the mechanism of power variations by constructing quasi-static solutions of the equivalent admittances of the arrays. The time factor $e^{j\omega t}$ will be omitted throughout.

2. STATEMENT OF THE PROBLEM

As illustrated in Figs. 1(a), (b), an infinite number of disks and circular apertures having radius a are allocated in the xy plane with the period d in both x and y directions. The disk array and the perforated sheet are made of noble-metal film with thickness b ($|z| < b/2$) and relative permittivity ε_r. They are free-standing in the air with electric constants ε_0 and μ_0. A plane wave $(\mathbf{E}^i, \mathbf{H}^i)$ is incident with the polar angle θ^i and the azimuth angle ϕ^i as shown in Fig. 1(c). The wavenumber vector, propagation constants, and wave impedance are given by

$$\begin{cases} \mathbf{k}^i = \mathbf{i}_x \alpha_0 + \mathbf{i}_y \beta_0 + \mathbf{i}_z \gamma_{00}, & \alpha_0 = k_0 \sin\theta^i \cos\phi^i, & \beta_0 = k_0 \sin\theta^i \sin\phi^i, & \gamma_{00} = k_0 \cos\theta^i \\ k_0 = \omega\sqrt{\varepsilon_0\mu_0} = 2\pi/\lambda, & \zeta_0 = \sqrt{\mu_0/\varepsilon_0} \end{cases} \quad (1)$$

where λ is wavelength, and $\mathbf{i}_w$ ($w = x, y, z$) is the unit vector parallel to the w axis. The periodicity of the system allows us to consider only over one unit cell, say, $|x| < d/2$ and $|y| < d/2$.
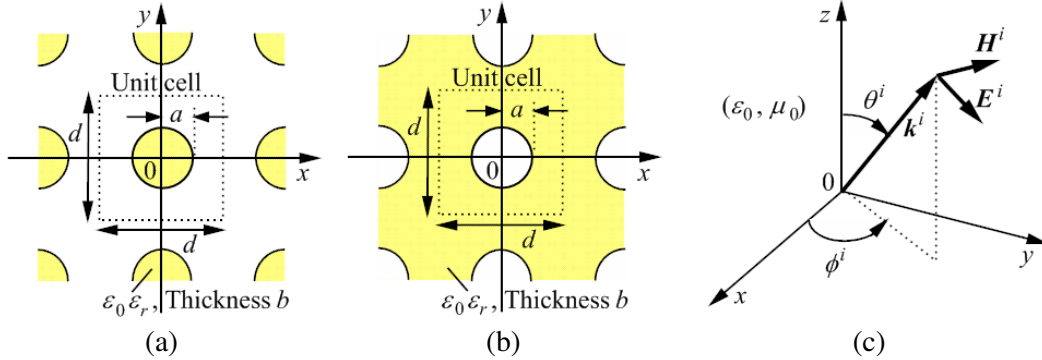

Figure 1. Geometry of the problem. (a) Two-dimensional periodic array of disks. (b) Array of circular apertures in an infinite sheet perforated complementarily to (a). (c) Incident plane wave.

Let us decompose the total electromagnetic field as $(\mathbf{E}, \mathbf{H}) = (\mathbf{E}^p, \mathbf{H}^p) + (\mathbf{E}^s, \mathbf{H}^s)$, where the superscripts p and s concern the primary and scattered (or secondary) fields, respectively. The former field is defined as follows.

- For the disk problem, $(\mathbf{E}^p, \mathbf{H}^p)$ is equal to $(\mathbf{E}^i, \mathbf{H}^i)$ for $|z| > b/2$, corresponding to the total field without disks.
- For the aperture problem, we write

$$(\mathbf{E}^p, \mathbf{H}^p) = \begin{cases} (\mathbf{E}^t, \mathbf{H}^t) & (z > b/2) \\ (\mathbf{E}^i, \mathbf{H}^i) + (\mathbf{E}^r, \mathbf{H}^r) & (z < -b/2) \end{cases} \quad (2)$$

where the superscripts t and r concern the transmitted and reflected plane waves, respectively, corresponding to the total field for an infinite sheet without perforation.

If the metal is electrically very thin ($b \ll \lambda$) and gives a high contrast to the air ($|\varepsilon_r| \gg 1$), we may impose the generalized boundary conditions [8] on the reduced surfaces $z = \pm 0$ as

$$\begin{cases} (1/2)\mathbf{i}_z \times [\mathbf{E}(x, y, +0) + \mathbf{E}(x, y, -0)] = R\mathbf{i}_z \times \mathbf{i}_z \times [\mathbf{H}(x, y, +0) - \mathbf{H}(x, y, -0)] \\ (1/2)\mathbf{i}_z \times [\mathbf{H}(x, y, +0) + \mathbf{H}(x, y, -0)] = -Q\mathbf{i}_z \times \mathbf{i}_z \times [\mathbf{E}(x, y, +0) - \mathbf{E}(x, y, -0)] \end{cases} \quad (3)$$

where the electric resistance and magnetic conductance are given by

$$R = \frac{\zeta_0}{j2\sqrt{\varepsilon_r}} \cot \frac{k_0 b\sqrt{\varepsilon_r}}{2}, \quad Q = \frac{\sqrt{\varepsilon_r}}{j2\zeta_0} \cot \frac{k_0 b\sqrt{\varepsilon_r}}{2} \tag{4}$$

For perfect conductors they are reduced to $R = 0$ and $|Q| \to \infty$.

3. DERIVATION OF THE INTEGRAL EQUATIONS

3.1. Field Expansion

The incident, transmitted, and reflected plane waves are written as

$$
\begin{pmatrix} \mathbf{E}^i & \mathbf{E}^t \\ \zeta_0 \mathbf{H}^i & \zeta_0 \mathbf{H}^t \end{pmatrix}
$$
$$
= \begin{pmatrix} \boldsymbol{\Psi}_{100}(x,y) & \boldsymbol{\Psi}_{200}(x,y) - \zeta_0 \eta_{200} \boldsymbol{\Psi}_{00}^z(x,y) \\ \zeta_0 \eta_{100} \boldsymbol{\Psi}_{200}(x,y) - \boldsymbol{\Psi}_{00}^z(x,y) & -\zeta_0 \eta_{200} \boldsymbol{\Psi}_{100}(x,y) \end{pmatrix} \begin{pmatrix} V_1 & A_1 \\ V_2 & A_2 \end{pmatrix} e^{-j\gamma_{00}z} \tag{5}
$$

$$
\begin{pmatrix} \mathbf{E}^r \\ \zeta_0 \mathbf{H}^r \end{pmatrix}
$$
$$
= \begin{pmatrix} \boldsymbol{\Psi}_{100}(x,y) & \boldsymbol{\Psi}_{200}(x,y) + \zeta_0 \eta_{200} \boldsymbol{\Psi}_{00}^z(x,y) \\ -\zeta_0 \eta_{100} \boldsymbol{\Psi}_{200}(x,y) - \boldsymbol{\Psi}_{00}^z(x,y) & \zeta_0 \eta_{200} \boldsymbol{\Psi}_{100}(x,y) \end{pmatrix} \begin{pmatrix} B_1 \\ B_2 \end{pmatrix} e^{j\gamma_{00}z} \tag{6}
$$

and the scattered field is expressed in the form of a superposition of the Floquet modes as [12–18]

$$
\begin{pmatrix} \mathbf{E}^s \\ \zeta_0 \mathbf{H}^s \end{pmatrix} = \sum_{p=-\infty}^{\infty} \sum_{q=-\infty}^{\infty}
$$
$$
\cdot \begin{cases} \begin{pmatrix} \boldsymbol{\Psi}_{1pq}(x,y) & \boldsymbol{\Psi}_{2pq}(x,y) - \zeta_0 \eta_{2pq} \boldsymbol{\Psi}_{pq}^z(x,y) \\ \zeta_0 \eta_{1pq} \boldsymbol{\Psi}_{2pq}(x,y) - \boldsymbol{\Psi}_{pq}^z(x,y) & -\zeta_0 \eta_{2pq} \boldsymbol{\Psi}_{1pq}(x,y) \end{pmatrix} \begin{pmatrix} A_{1pq} \\ A_{2pq} \end{pmatrix} e^{-j\gamma_{pq}z} & (z > 0) \\[1em]
\begin{pmatrix} \boldsymbol{\Psi}_{1pq}(x,y) & \boldsymbol{\Psi}_{2pq}(x,y) + \zeta_0 \eta_{2pq} \boldsymbol{\Psi}_{pq}^z(x,y) \\ -\zeta_0 \eta_{1pq} \boldsymbol{\Psi}_{2pq}(x,y) - \boldsymbol{\Psi}_{pq}^z(x,y) & \zeta_0 \eta_{2pq} \boldsymbol{\Psi}_{1pq}(x,y) \end{pmatrix} \begin{pmatrix} B_{1pq} \\ B_{2pq} \end{pmatrix} e^{j\gamma_{pq}z} & (z < 0) \end{cases} \tag{7}
$$

where the vector mode functions are

$$
\begin{pmatrix} \boldsymbol{\Psi}_{1pq}(x,y) \\ \boldsymbol{\Psi}_{2pq}(x,y) \\ \boldsymbol{\Psi}_{pq}^z(x,y) \end{pmatrix} = \begin{pmatrix} \beta_q \mathbf{i}_x - \alpha_p \mathbf{i}_y \\ \alpha_p \mathbf{i}_x + \beta_q \mathbf{i}_y \\ (\alpha_p^2 + \beta_q^2)\,\mathbf{i}_z/k \end{pmatrix} \frac{e^{-j(\alpha_p x + \beta_q y)}}{\sqrt{\alpha_p^2 + \beta_q^2}\, d} \tag{8}
$$

with the propagation constants and mode admittances

$$
\begin{cases} \alpha_p = \alpha_0 + 2p\pi/d, & \beta_q = \beta_0 + 2q\pi/d, & \gamma_{pq} = \left(k_0^2 - \alpha_p^2 - \beta_q^2\right)^{1/2} & (\mathrm{Im}\,\gamma_{pq} \le 0) \\ \eta_{1pq} = \gamma_{pq}/(\zeta_0 k_0), & \eta_{2pq} = k_0/(\zeta_0 \gamma_{pq}) \end{cases} \tag{9}
$$

The mode functions satisfy the periodicity condition $\Psi(x + pd, y + qd) = \Psi(x,y)e^{-j(p\alpha_0 + q\beta_0)d}$ (Ψ: arbitrary component) as well as the orthonormal property

$$
\int_{-d/2}^{d/2} \int_{-d/2}^{d/2} \boldsymbol{\Psi}_{spq}(x,y) \cdot \boldsymbol{\Psi}_{s'p'q'}^*(x,y)\, dx\, dy = \delta_{ss'} \delta_{pp'} \delta_{qq'} \tag{10}
$$

where the asterisk denotes complex conjugate and $\delta_{ss'}$ is Kronecker's delta. Owing to the periodicity condition, the coupling among unit cells is automatically incorporated in the analysis. If this periodic nature is violated, we must deal with the whole structure governed by infinite space Green's functions. Still in some cases having partial periodicity, transformation process may be be valid [16].

The coefficients in (5)–(7) are explained as follows.

- For the incident field in (5), the voltage constants are given by $V_1 = -V_0 \cos \delta^i$ and $V_2 = V_0 \cos \theta^i \sin \delta^i$ where $|\mathbf{E}^i| = V_0/d$. The angle δ^i stands for polarization, with $\delta^i = 0$ and $\delta^i = \pi/2$ corresponding to the TE and TM waves, respectively, with respect to the z axis.

- For the transmitted and reflected plane waves by an infinite sheet, substitution of (5) and (6) into the boundary conditions (3) yields

$$
\begin{pmatrix} A_s \\ B_s \end{pmatrix} = \left(-\frac{1 - 2R\eta_{s00}}{1 + 2R\eta_{s00}} \mp \frac{1 - 2Q/\eta_{s00}}{1 + 2Q/\eta_{s00}} \right) \frac{V_s}{2} \quad (s = 1 : \text{TE}, \, s = 2 : \text{TM}) \tag{11}
$$

The exact expression for (11) is given in Appendix A. Note that the above constants are not employed in the disk problem of Fig. 1(a).

- The constants A_{spq} and B_{spq} in (7) are the unknown transmission and reflection coefficients, respectively, of the pq-th mode.

3.2. Integral Equations for the Disk Problem

As we have observed, some differences in the solution process arise between the disk and aperture problems. Let us first concentrate our attention to the former problem. Unknown functions are the surface electric and magnetic current densities induced on the disk which are defined by

$$
\left.\begin{array}{l} \mathbf{J}(x, y) = \mathbf{i}_z \times [\mathbf{H}(x, y, +0) - \mathbf{H}(x, y, -0)] \\ \mathbf{M}(x, y) = -\mathbf{i}_z \times [\mathbf{E}(x, y, +0) - \mathbf{E}(x, y, -0)] \end{array}\right\} \quad (|x| < d/2, \, |y| < d/2) \tag{12}
$$

Since the incident field is continuous everywhere, we are allowed to replace $(\mathbf{E}, \mathbf{H})$ in (12) with $(\mathbf{E}^s, \mathbf{H}^s)$. We substitute the scattered field (7) into (12), take the dot product with $\mathbf{\Psi}^*_{s'p'q'}(x, y)$, and integrate it over the unit cell. The orthogonality (10) permits us to leave only one term out of the infinite sums $\sum_{p,q}$. Due to the field continuity on the xy plane except the disk part that

$$
\mathbf{J}(x, y) = \mathbf{M}(x, y) = 0 \quad \left(|x| < d/2, \, |y| < d/2, \, \sqrt{x^2 + y^2} > a \right) \tag{13}
$$

one can reduce the integration range from the square unit cell to the circular disk surface. Consequently, we arrive at the integral representations of the mode coefficients

$$
\left\{ \begin{array}{l} \begin{pmatrix} A_{1pq} \\ B_{1pq} \end{pmatrix} = \dfrac{1}{2} \iint\limits_{\sqrt{x^2+y^2}<a} \left[-\dfrac{1}{\eta_{1pq}} \mathbf{J}(x, y) \cdot \mathbf{\Psi}^*_{1pq}(x, y) \mp \mathbf{M}(x, y) \cdot \mathbf{\Psi}^*_{2pq}(x, y) \right] dx dy \\[3mm] \begin{pmatrix} A_{2pq} \\ B_{2pq} \end{pmatrix} = \dfrac{1}{2} \iint\limits_{\sqrt{x^2+y^2}<a} \left[-\dfrac{1}{\eta_{2pq}} \mathbf{J}(x, y) \cdot \mathbf{\Psi}^*_{2pq}(x, y) \pm \mathbf{M}(x, y) \cdot \mathbf{\Psi}^*_{1pq}(x, y) \right] dx dy \end{array}\right. \tag{14}
$$

Let us derive the integral equations by expressing the boundary conditions (3) in terms of surface current densities $\mathbf{J}$ and $\mathbf{M}$. The left and right hand sides of (3) are treated as follows.

Left hand side The expressions of (5) and (7) are substituted, and then the coefficients A_{sqp} and B_{spq} are converted to integral forms by means of (14) that includes the current densities.

Right hand side It is straightforwardly written by using $\mathbf{J}$ and $\mathbf{M}$ with the aid of (12).

The above procedure leads us to the set of integral equations

$$
\begin{pmatrix} R\mathbf{J}(x, y) \\ \zeta_0^2 Q\mathbf{M}(x, y) \end{pmatrix} + \sum_{s=1}^{2} \sum_{p=-\infty}^{\infty} \sum_{q=-\infty}^{\infty} \frac{1}{2\eta_{spq}} \mathbf{\Psi}_{spq}(x, y) \iint\limits_{\sqrt{x'^2+y'^2}<a} \begin{pmatrix} \mathbf{J}(x', y') \\ \mathbf{M}(x', y') \end{pmatrix} \cdot \mathbf{\Psi}^*_{spq}(x', y') dx' dy'
$$
$$
= \begin{pmatrix} \mathbf{\Psi}_{100}(x, y) & \mathbf{\Psi}_{200}(x, y) \\ \mathbf{\Psi}_{200}(x, y)/\eta_{200} & -\mathbf{\Psi}_{100}(x, y)/\eta_{100} \end{pmatrix} \begin{pmatrix} V_1 \\ V_2 \end{pmatrix} \quad \left(\sqrt{x^2 + y^2} < a \right) \tag{15}
$$

where $\mathbf{J}$ and $\mathbf{M}$ are uncoupled.

3.3. Integral Equations for the Aperture Problem

The process is nearly parallel to the disk case, but the unknown functions should be redefined by

$$
\left.\begin{array}{l} \mathbf{M}(x, y) = (-1/2)\mathbf{i}_z \times [\mathbf{E}(x, y, +0) + \mathbf{E}(x, y, -0)] + R\mathbf{i}_z \times \mathbf{i}_z \times [\mathbf{H}(x, y, +0) - \mathbf{H}(x, y, -0)] \\ \mathbf{J}(x, y) = (1/2)\mathbf{i}_z \times [\mathbf{H}(x, y, +0) + \mathbf{H}(x, y, -0)] + Q\mathbf{i}_z \times \mathbf{i}_z \times [\mathbf{E}(x, y, +0) - \mathbf{E}(x, y, -0)] \end{array}\right\}
$$
$$
(|x| < d/2, \, |y| < d/2) \tag{16}
$$

Note that these are not true current densities but equivalent ones. This choice makes the vanishment condition (13) still hold for the metal part. Following to the routine, we are led to the integral representation of the mode coefficients

$$
\begin{cases}
\begin{pmatrix} A_{1pq} \\ B_{1pq} \end{pmatrix} = \iint_{\sqrt{x^2+y^2}<a} \left[-\frac{\mathbf{M}(x,y) \cdot \mathbf{\Psi}^*_{2pq}(x,y)}{1+2R\eta_{1pq}} \mp \frac{\mathbf{J}(x,y) \cdot \mathbf{\Psi}^*_{1pq}(x,y)}{\eta_{1pq}+2Q} \right] dxdy \\
\begin{pmatrix} A_{2pq} \\ B_{2pq} \end{pmatrix} = \iint_{\sqrt{x^2+y^2}<a} \left[\frac{\mathbf{M}(x,y) \cdot \mathbf{\Psi}^*_{1pq}(x,y)}{1+2R\eta_{2pq}} \mp \frac{\mathbf{J}(x,y) \cdot \mathbf{\Psi}^*_{2pq}(x,y)}{\eta_{2pq}+2Q} \right] dxdy
\end{cases}
\tag{17}
$$

and the set of integral equations

$$
\sum_{s=1}^{2} \sum_{p=-\infty}^{\infty} \sum_{q=-\infty}^{\infty} \mathbf{\Psi}_{spq}(x,y) \iint_{\sqrt{x'^2+y'^2}<a} \begin{pmatrix} \mathbf{M}(x',y')/(\zeta_0\eta_{spq}+2R/\zeta_0) \\ \mathbf{J}(x',y')/(\eta_{spq}+2Q) \end{pmatrix} \cdot \mathbf{\Psi}^*_{spq}(x',y') \, dx' dy'
$$

$$
= \begin{pmatrix} V_2/(\zeta_0\eta_{100}+2R/\zeta_0) & -V_1/(\zeta_0\eta_{200}+2R/\zeta_0) \\ -V_1/(1+2Q/\eta_{100}) & -V_2/(1+2Q/\eta_{200}) \end{pmatrix} \begin{pmatrix} \mathbf{\Psi}_{100}(x,y) \\ \mathbf{\Psi}_{200}(x,y) \end{pmatrix} \quad \left(\sqrt{x^2+y^2} < a \right)
\tag{18}
$$

where R and Q always appear together with η_{spq}.

4. METHOD OF MOMENTS

4.1. Disk Problem

Let us solve the integral Equation (15) numerically for the disk problem by means of the method of moments [19]. As a first step, we approximate the unknown functions by finite sums as

$$
\begin{pmatrix} \zeta_0\mathbf{J}(x,y) \\ \mathbf{M}(x,y) \end{pmatrix} \approx \sum_{t=1}^{2} \sum_{m=-M}^{M} \sum_{n=1}^{N} \begin{pmatrix} F^J_{tmn} \\ F^M_{tmn} \end{pmatrix} \mathbf{\Phi}_{tmn}(r,\phi) \quad (0 < r < a, \ -\pi < \phi < \pi)
\tag{19}
$$

where the cylindrical coordinate system is introduced by $x = r\cos\phi$ and $y = r\sin\phi$. The basis functions are constructed from $\mathbf{\Phi}_{1mn} \propto \nabla_T \psi_{1mn}$ and $\mathbf{\Phi}_{2mn} \propto \nabla_T \times (\psi_{2mn}\mathbf{i}_z)$, where the potential ψ_{tmn} ($t = 1, 2$) is a solution of the two-dimensional Helmholtz equation $(\nabla_T^2 + k_{tmn}^2)\psi_{tmn}(r,\phi) = 0$. Suitable eigenvalues and eigenfunctions are $k_{1mn} = \xi'_{mn}/a$, $k_{2mn} = \xi_{mn}/a$, and $\psi_{tmn} = J_m(k_{tmn}r)e^{jm\phi}$, from which we obtain

$$
\begin{cases}
\mathbf{\Phi}_{1mn}(r,\phi) = \frac{f_{1mn}}{a} \left[J'_m\left(\frac{\xi'_{mn}}{a}r\right) \mathbf{i}_r + \frac{jma}{\xi'_{mn}r} J_m\left(\frac{\xi'_{mn}}{a}r\right) \mathbf{i}_\phi \right] e^{jm\phi} \\
\mathbf{\Phi}_{2mn}(r,\phi) = \frac{f_{2mn}}{a} \left[\frac{ma}{j\xi_{mn}r} J_m\left(\frac{\xi_{mn}}{a}r\right) \mathbf{i}_r + J'_m\left(\frac{\xi_{mn}}{a}r\right) \mathbf{i}_\phi \right] e^{jm\phi} \\
f_{1mn} = \frac{\xi'_{mn}}{\sqrt{\pi(\xi'^2_{mn}-m^2)}J_m(\xi'_{mn})}, \quad f_{2mn} = \frac{1}{\sqrt{\pi}J'_m(\xi_{mn})}
\end{cases}
\tag{20}
$$

where the symbols ξ_{mn} and ξ'_{mn} are the n-th zeros of the Bessel function $J_m(x)$ and its derivative $J'_m(x)$, respectively. Note that the combination of (19) and (20) exhibits proper edge behavior of the current that $(J_r, M_r) \to 0$ and $(J_\phi, M_\phi) < \infty$ as $r \to a$, if not exact up to the order [20]. An opposite choice of ψ_{1mn} and ψ_{2mn} would violate this condition. Owing to the normalization constants f_{tmn} ($t = 1, 2$), we have the orthonormal property

$$
\int_{-\pi}^{\pi} \int_0^a \mathbf{\Phi}_{tmn}(r,\phi) \cdot \mathbf{\Phi}^*_{t'm'n'}(r,\phi) r dr d\phi = \delta_{tt'} \delta_{mm'} \delta_{nn'}
\tag{21}
$$

We further note that the functions (20) with real eigenvalues may be used to describe transmission modes in circular waveguides homogeneously filled with not only lossless but also lossy materials.

As a second step of the method of moments, we substitute (19) into (15), take the dot product with the testing function $\mathbf{\Phi}^*_{tmn}(r,\phi)$ ($t = 1, 2$; $m = 0, \pm 1, \ldots, \pm M$; $n = 1, 2, \ldots, N$), and integrate it

over the disk surface $r < a$. Employment of (21) leads us to the set of linear equations

$$\begin{pmatrix} (R/\zeta_0)F_{tmn}^J \\ Q\zeta_0 F_{tmn}^M \end{pmatrix} + \sum_{t'=1}^{2}\sum_{m'=-M}^{M}\sum_{n'=1}^{N} K_{tmn,t'm'n'} \begin{pmatrix} F_{t'm'n'}^J \\ F_{t'm'n'}^M \end{pmatrix} = \begin{pmatrix} G_{tmn}^J \\ G_{tmn}^M \end{pmatrix}$$

$$(t = 1, 2; \ m = 0, \pm 1, \ldots, \pm M; \ n = 1, 2, \ldots, N) \tag{22}$$

where the system and driving elements are written as

$$\begin{cases} K_{tmn,t'm'n'} = \sum_{s=1}^{2}\sum_{p=-P}^{P}\sum_{q=-P}^{P} \frac{1}{2\zeta_0\eta_{spq}} C_{tmn,spq}^* C_{t'm'n',spq} \\[2ex] \begin{pmatrix} G_{tmn}^J \\ G_{tmn}^M \end{pmatrix} = \begin{pmatrix} C_{tmn,100}^* & C_{tmn,200}^* \\ C_{tmn,200}^*/(\zeta_0\eta_{200}) & -C_{tmn,100}^*/(\zeta_0\eta_{100}) \end{pmatrix} \begin{pmatrix} V_1 \\ V_2 \end{pmatrix} \end{cases} \tag{23}$$

with infinite sums $\sum_{p,q}$ truncated at $\pm P$, and the inner product is defined by

$$C_{tmn,spq} = \int_{-\pi}^{\pi}\int_{0}^{a} \mathbf{\Phi}_{tmn}(r, \phi) \cdot \mathbf{\Psi}_{spq}^*(x, y) r \, dr \, d\phi \tag{24}$$

We analytically evaluate this integral and give the results in Appendix B. The mode coefficients are obtained by substituting the numerical solution of (22) into

$$\begin{cases} \begin{pmatrix} A_{1pq} \\ B_{1pq} \end{pmatrix} = \frac{1}{2}\sum_{t=1}^{2}\sum_{m=-M}^{M}\sum_{n=1}^{N} \left[-\frac{1}{\zeta_0\eta_{1pq}}F_{tmn}^J C_{tmn,1pq} \mp F_{tmn}^M C_{tmn,2pq} \right] \\[2ex] \begin{pmatrix} A_{2pq} \\ B_{2pq} \end{pmatrix} = \frac{1}{2}\sum_{t=1}^{2}\sum_{m=-M}^{M}\sum_{n=1}^{N} \left[-\frac{1}{\zeta_0\eta_{2pq}}F_{tmn}^J C_{tmn,2pq} \pm F_{tmn}^M C_{tmn,1pq} \right] \end{cases} \tag{25}$$

4.2. Aperture Problem

The integral Equation (18) for the aperture problem are treated as follows. The first step in the method of moments is exactly the same as what has been done as (19) and (20). The second procedure is also similar, resulting in the set of linear equations

$$\sum_{t'=1}^{2}\sum_{m'=-M}^{M}\sum_{n'=1}^{N} \begin{pmatrix} K_{tmn,t'm'n'}^M F_{t'm'n'}^M \\ K_{tmn,t'm'n'}^J F_{t'm'n'}^J \end{pmatrix} = \begin{pmatrix} G_{tmn}^M \\ G_{tmn}^J \end{pmatrix} \quad (t = 1, 2; \ m = 0, \pm 1, \ldots, \pm M; \ n = 1, 2, \ldots, N) \tag{26}$$

where the known coefficients are written as

$$\begin{cases} \begin{pmatrix} K_{tmn,t'm'n'}^M \\ K_{tmn,t'm'n'}^J \end{pmatrix} = \sum_{s=1}^{2}\sum_{p=-P}^{P}\sum_{q=-P}^{P} \begin{pmatrix} 1/(\zeta_0\eta_{spq} + 2R/\zeta_0) \\ 1/(\zeta_0\eta_{spq} + 2Q\zeta_0) \end{pmatrix} C_{tmn,spq}^* C_{t'm'n',spq} \\[2ex] \begin{pmatrix} G_{tmn}^M \\ G_{tmn}^J \end{pmatrix} = \begin{pmatrix} V_2/(\zeta_0\eta_{100} + 2R/\zeta_0) & -V_1/(\zeta_0\eta_{200} + 2R/\zeta_0) \\ -V_1/(1 + 2Q/\eta_{100}) & -V_2/(1 + 2Q/\eta_{200}) \end{pmatrix} \begin{pmatrix} C_{tmn,100}^* \\ C_{tmn,200}^* \end{pmatrix} \end{cases} \tag{27}$$

with the inner product given by (24). Solving (26) numerically, we calculate the mode coefficients from

$$\begin{cases} \begin{pmatrix} A_{1pq} \\ B_{1pq} \end{pmatrix} = \sum_{t=1}^{2}\sum_{m=-M}^{M}\sum_{n=1}^{N} \left[-\frac{F_{tmn}^M C_{tmn,2pq}}{1 + 2R\eta_{1pq}} \mp \frac{F_{tmn}^J C_{tmn,1pq}}{(\eta_{1pq} + 2Q)\zeta_0} \right] \\[2ex] \begin{pmatrix} A_{2pq} \\ B_{2pq} \end{pmatrix} = \sum_{t=1}^{2}\sum_{m=-M}^{M}\sum_{n=1}^{N} \left[\frac{F_{tmn}^M C_{tmn,1pq}}{1 + 2R\eta_{2pq}} \mp \frac{F_{tmn}^J C_{tmn,2pq}}{(\eta_{2pq} + 2Q)\zeta_0} \right] \end{cases} \tag{28}$$

4.3. Choice of Truncation Numbers

The truncation numbers M, N, and P in (19), (23), and (27) must be suitably chosen with paying attention to the relative convergence phenomenon [21]. Seeing that a pair $(|m|, n)$ runs from $(0, 1)$ up to (M, N), it is appropriate to combine M and N so that the zeros ξ_{0N} and ξ_{M1} are roughly comparable. This is established in the leftmost two columns in Table 1. Letting the ratio of the number of harmonics assigned to a unit cell and a disk be approximately proportional to the ratio of their areas, we get

$$\frac{\displaystyle\sum_{m=-M}^{M}\sum_{n=1}^{N}1}{\displaystyle\sum_{p=-P}^{P}\sum_{q=-P}^{P}1} = \frac{(2M+1)N}{(2P+1)^2} \approx \frac{\pi a^2}{d^2} \qquad (29)$$

This relation is displayed in the rightmost two columns in Table 1. In the numerical computation, we first calculate $(2P+1)^2\pi a^2/d^2$ from a preset number P and given ratio a/d, and then select M and N listed in the corresponding row in Table 1.

Table 1. Relation among the truncation numbers M, N, and P.

M	N	$\xi_{0N} \approx \xi_{M1}$		$(2M+1)N \approx (2P+1)^2\pi a^2/d^2$	
1	2	5.520	3.832	6	0.0–8.0
2	2	5.520	5.136	10	8.0–12.0
3	2	5.520	6.380	14	12.0–20.5
4	3	8.654	7.588	27	20.5–30.0
5	3	8.654	8.771	33	30.0–36.0
6	3	8.654	9.936	39	36.0–49.5
7	4	11.79	11.09	60	49.5–64.0
8	4	11.79	12.23	68	64.0–81.5
9	5	14.93	13.35	95	81.5–100.0
10	5	14.93	14.48	105	100.0–

5. NUMERICAL RESULTS

5.1. Power Distributions

Figures 2(a), (b) show the total reflected power $\sum_{s,p,q} \eta_{spq}|B_{spq}|^2$ for disks, and Figs. 2(c), (d) is the total transmitted power $\sum_{s,p,q} \eta_{spq}|A_{spq} + A_s\delta_{p0}\delta_{q0}|^2$ for apertures, with normalized by the incident power $\cos\theta^i V_0^2/\zeta_0$. The sum $\sum_{p,q}$ extends over all the propagating modes for which $\mathrm{Re}\gamma_{pq} > 0$. Polarization of incidence is TE ($\delta^i = 0$, $E_z^i = 0$) and TM ($\delta^i = \pi/2$, $H_z^i = 0$) for (a), (c) and (b), (d), respectively. When setting the permittivity of materials as a function of wavelength λ, we carried out the Spline interpolation into the discrete experimental values presented by [22]. The thickness b is taken equal to the skin depth at $\lambda = 800\,\mathrm{nm}$. Data for perfect electric conductor (PEC), though fictitious in the optical range, is added only for reference. The curves tell the following features.

All metals The powers rapidly change near the Rayleigh wavelengths $\lambda = 232\,\mathrm{nm}$ and $410\,\mathrm{nm}$, at which the $(-1, \pm 1)$-th and $(-1, 0)$-th modes, respectively, are cutoff. This concerns what is called the grating resonance. Though such change in the reflected power is hardly seen at $\lambda = 410\,\mathrm{nm}$ for gold in (b), we have verified distinguishable fluctuations for the transmitted and absorbed powers.

PEC The characteristics in (a) and (d) are identical due to Babinet's principle for complementary structures. The same applies to (b) and (c).
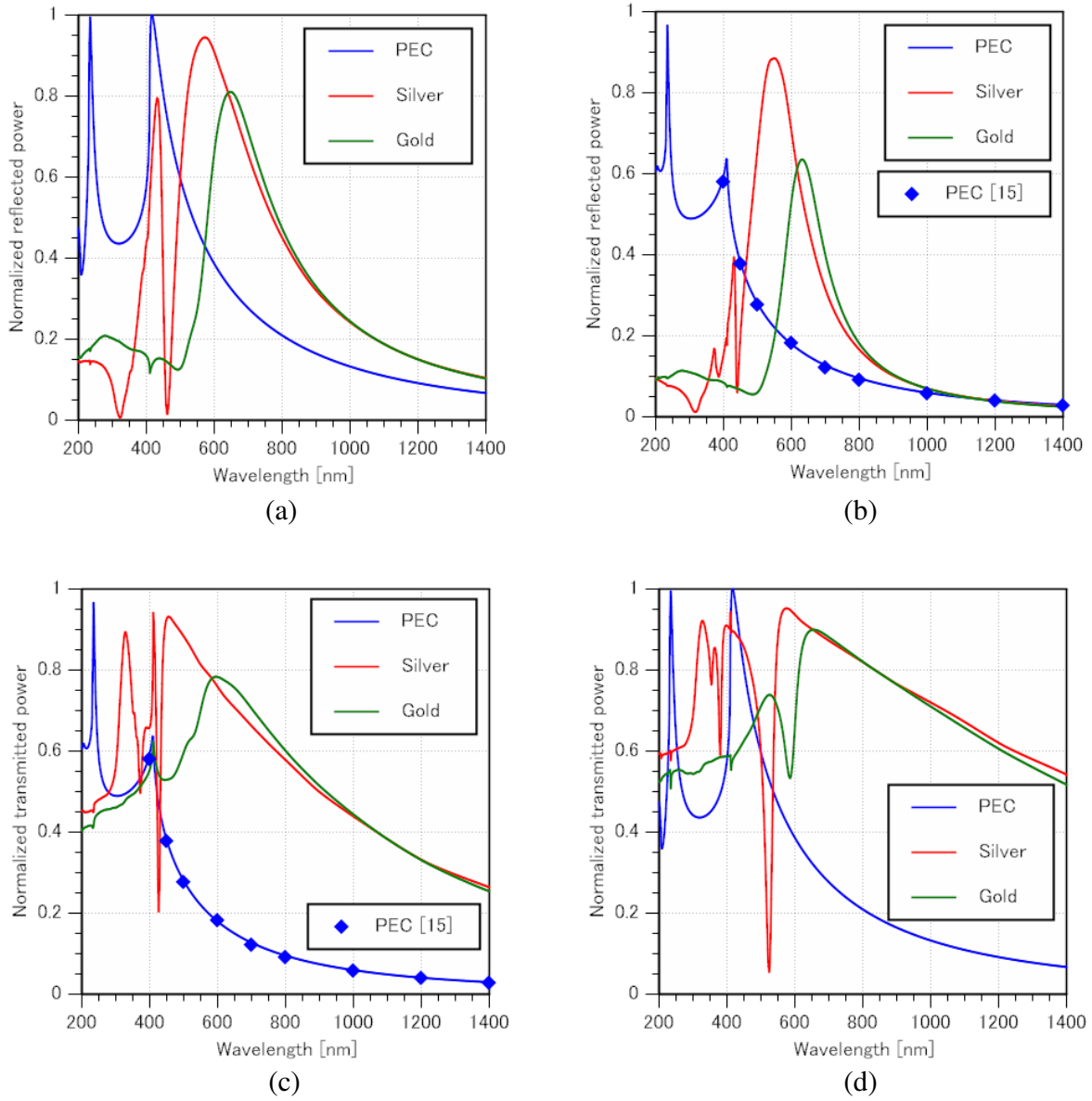
Figure 2. Normalized values of total reflected and transmitted powers as a function of wavelength λ. The size is given by $d = 240\,\mathrm{nm}$, $a = 100\,\mathrm{nm}$, and $b = 0$ (PEC), $23\,\mathrm{nm}$ (silver), and $26\,\mathrm{nm}$ (gold). The incident angles are $\theta^i = 45°$ and $\phi^i = 0$. (a) Reflected power for a disk array at TE incidence. (b) Same as (a) but TM incidence. (c) Transmitted power for an aperture array at TE incidence. (d) Same as (c) but TM incidence.

Silver In the vicinity of $\lambda = 320\,\mathrm{nm}$, a minimum and a maximum appear for disks (a), (b) and apertures (c), (d), respectively. This is because $\varepsilon_r = 0.363 - j0.5470$ at $\lambda = 322\,\mathrm{nm}$, at which the skin depth is $134\,\mathrm{nm}$ $(\gg b)$ and then the scattering effect becomes weak.

Silver and gold Maxima and minima appear in the long wave range $\lambda > 400\,\mathrm{nm}$. This will be discussed in **5.2** in association with the quasi-static solution. The peak of transmitted power for apertures is a lot to do with the extraordinary optical transmission phenomenon.

On the whole, the amount of reflection (transmission) is larger in the TE (TM) case compared with the TM (TE) case, especially when the wavelength is long. This property originates from the shield

against the incident electric field (the surface current excitation by the incident magnetic field).

The marks in Figs. 2(b), (c) for PEC are taken from the data of Fig. 12 in [15] based on the generalized sheet transition condition (GSTC) approach. Since [15] dealt with microwave frequencies, we scaled the scatterer size and wavelength both 2×10^{-5} times in order to adjust to the optical range. The coefficients of reflection and transmission are squared to yield powers. Good agreement is observed.

We hereafter confine ourself to silver structures at normal incidence. Fig. 3 shows total reflected and transmitted powers for the arrays of disks and apertures, respectively, at a fixed ratio of radius to period. The thickness (the period) is common to Figs. 3(a), (b) (Figs. 3(c), (d)). The features are as follows.

- Grating resonance occurs when higher order modes become cutoff. Since the unit cell is square and the incidence is normal, the sets of four modes degenerate in the following manner.
  - Cutoff condition of the $(0, \pm 1)$-th and $(\pm 1, 0)$-th modes is presented by the relation $d = \lambda$. The gradient of this straight line is unity in (a), (b) and infinity in (c), (d). We clearly recognize such traces on each map.
  - The modes numbered by $(\pm 1, \pm 1)$, $(0, \pm 2)$, and $(\pm 2, 0)$ get cutoff on the lines $d = \sqrt{2}\lambda$ and $d = 2\lambda$. The corresponding traces along them are, however, vague or indistinctive.
- As seen from (c), (d), the power variation becomes stable when the thickness exceeds the skin depth. This means that the metal surface plays a dominant role in the phenomenon.
- Low reflection in (a), (c) and high transmission in (b), (d) are observed as vertical stripes around $\lambda \approx 320$ nm in each map. For apertures (b), (d), another two regions of high transmission appear in the single mode range $\lambda > d$. The same kind of behavior was also seen in Fig. 2.

Figure 4 shows the absorbed power for three different sizes of radius at a fixed period and thickness. The power for a disk array is found from $\mathrm{Re} \iint_{r<a} (R|\mathbf{J}|^2 + Q|\mathbf{M}|^2) dS$, and after combined with (19) and (21), we get $\mathrm{Re} \sum_{t,m,n} [(R/\zeta_0)|F_{tmn}^J|^2 + Q\zeta_0|F_{tmn}^M|^2]$. In the case of apertures, however, the surface integration is difficult to perform because of the irregularity of the metal shape that $r > a$ and $|x|$, $|y| < d/2$. This decides us to identify the absorbed power by subtracting the transmitted and reflected ones from the incident one. The features of Fig. 4 are stated as follows.

- For both arrays, the absorbed power in the short wave range $\lambda < 300$ nm increases as the area occupied by the metal becomes large. In the case of apertures with 50 nm-radius, the normalized absorbed power is 0.572 at $\lambda = 250$ nm, which is close to the value for an infinite sheet, i.e., 0.580.
- We observe a lot of spikes at the Rayleigh wavelengths 250 nm, 354 nm, and 500 nm, besides other wavelengths. A prominent peak occurs near 600 nm for contacting large disks ($a = 250$ nm) and small apertures ($a = 50$ nm), which may be due to the grating resonance and the propagation loss of excited surface waves. Another peak is found for small disks ($a = 50$ nm) stemming from the periodicity effect along with strong interactions among scattered modes. This phenomenon in the single mode range $\lambda > 500$ nm will be discussed in **5.2** with the aid of the quasi-static solution.

Before concluding the present subsection, we make some remarks on the convergence of solution. Fig. 5(a) shows the normalized transmitted, reflected, and absorbed powers, in addition to the sum of them, for a gold disk array treated in Fig. 2(a). We verify the law of power conservation that the incident power is equal to a total of these distributed powers, which has been discussed in waveguide discontinuity problems [23]. The truncation numbers are chosen as $P = 5$, $M = 8$, and $N = 4$, and its sufficiency is understood when observing Fig. 2(b). The four filled circles correspond to the appropriate pair of M and N determined by the criterion in Table 1 for $P = 1, 3, 5$, and 7. We see that the solution becomes stable when P reaches 5.

5.2. Quasi-Static Solution

As we have seen in **5.1**, the powers for silver and gold arrays get abrupt changes at wavelengths still longer than the longest Rayleigh wavelength, which is not observed for PEC. Though the extraordinary optical transmission was studied for a plate as thick as 200 nm with periodic perforation [6], it is enough suggestive also for thin plates to be considered analytically as was done in [14, 24]. Let us take note of
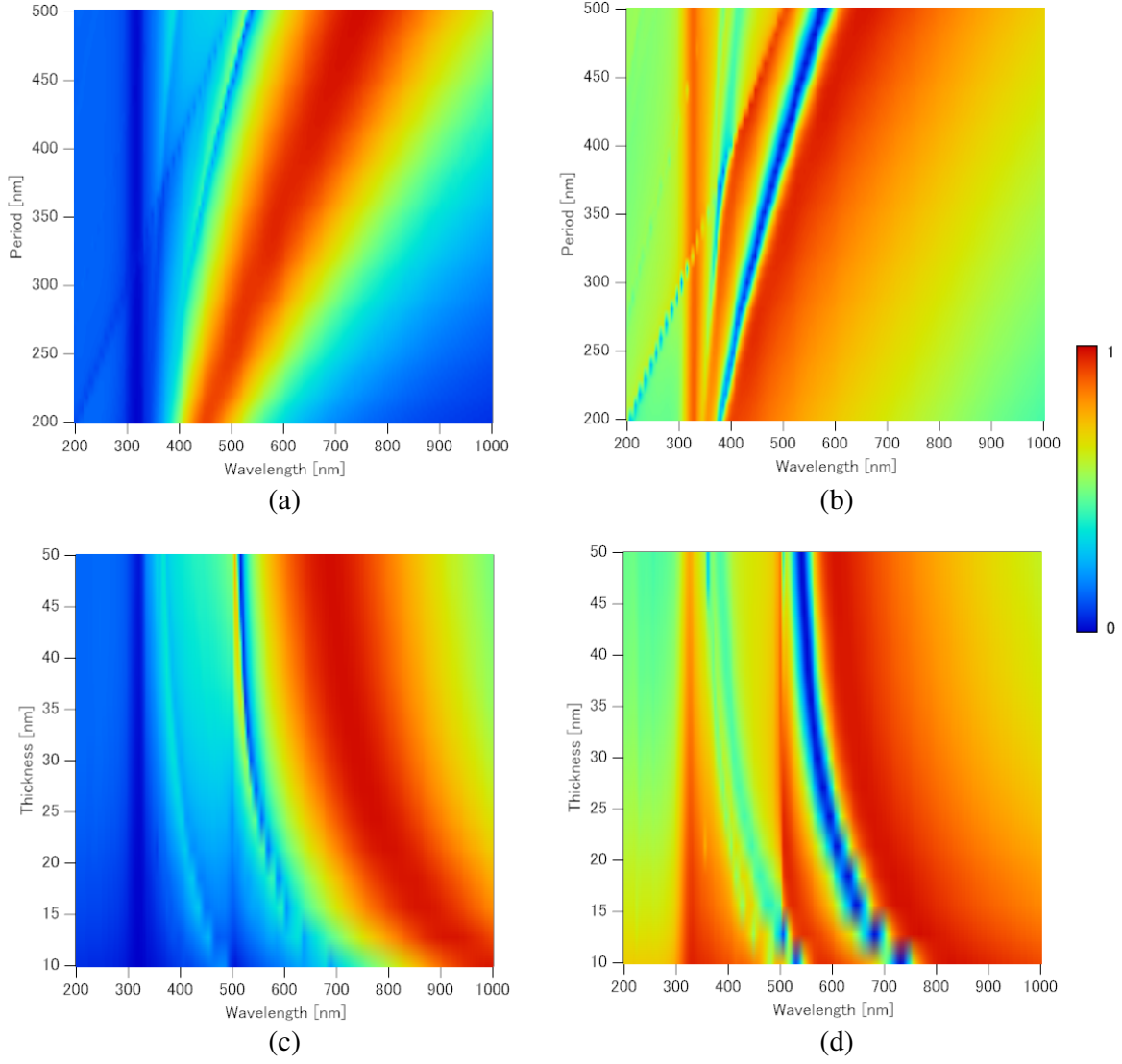
Figure 3. Normalized powers for silver arrays at normal incidence $\theta^i = \phi^i = 0$ as a function of wavelength λ, period d, and thickness b. The ratio a/d is fixed at 0.4. (a) Reflected power for disks with $b = 30$ nm. (b) Transmitted power for apertures with $b = 30$ nm. (c) Reflected power for disks with $d = 500$ nm. (d) Transmitted power for apertures with $d = 500$ nm.

this feature based on the quasi-static solution that is effective at low frequencies. For simplicity, we will treat only the case of normal incidence ($\theta^i = \phi^i = 0$) of the TEM wave (reduced TM wave, $\delta^i = \pi/2$).

Taking account of the lowest zero for the Bessel functions, $\xi'_{11} = 1.841$, we retain only F^J_{1m1} and F^M_{1m1} ($m = \pm 1$) from (19). Thereby the linear Equations (22) and (26) are solved by division. By setting as $P = 1$ in (23) and (27), the transmission and reflection coefficients of the dominant mode become

$$
A_{100} = B_{100} = 0, \quad \begin{pmatrix} A_{200} \\ B_{200} \end{pmatrix} = \begin{cases} \left(-\dfrac{1}{1 + 1/\bar{Y}^J} \mp \dfrac{1}{1 + \bar{Y}^M} \right) V_0 & \text{(disks)} \\[4mm] \left(\dfrac{1}{1 + 1/\bar{Y}^M} \pm \dfrac{1}{1 + \bar{Y}^J} \right) V_0 & \text{(apertures)} \end{cases} \tag{30}
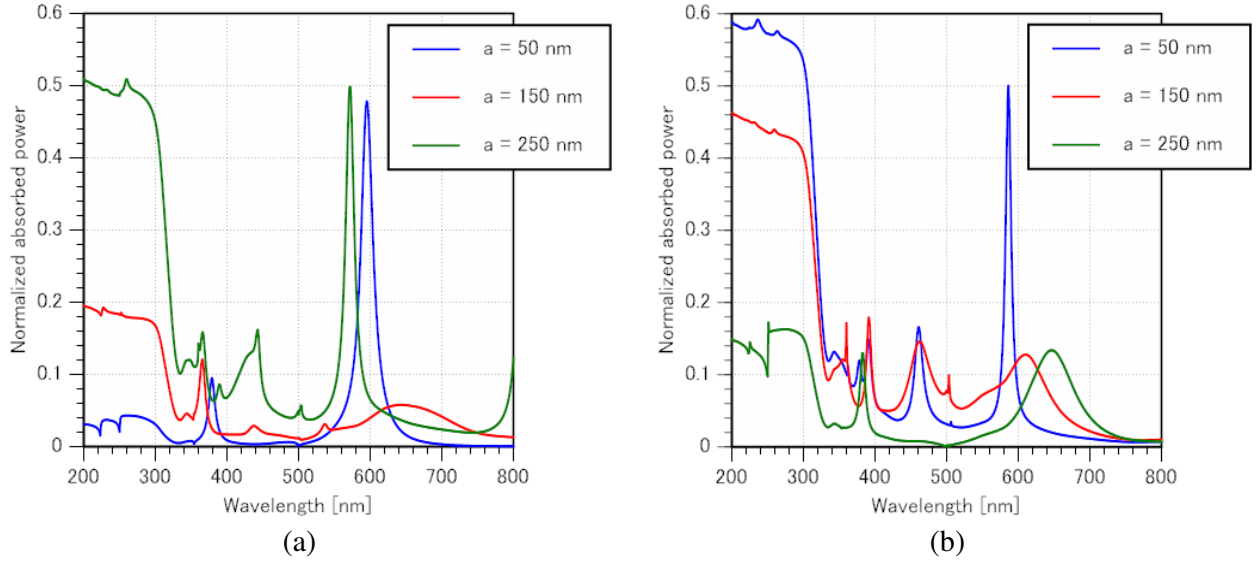$$

Figure 4. Normalized absorbed power for silver arrays at normal incidence. The size is given by $d = 500\,\text{nm}$ and $b = 30\,\text{nm}$. (a) Array of disks. (b) Array of apertures.
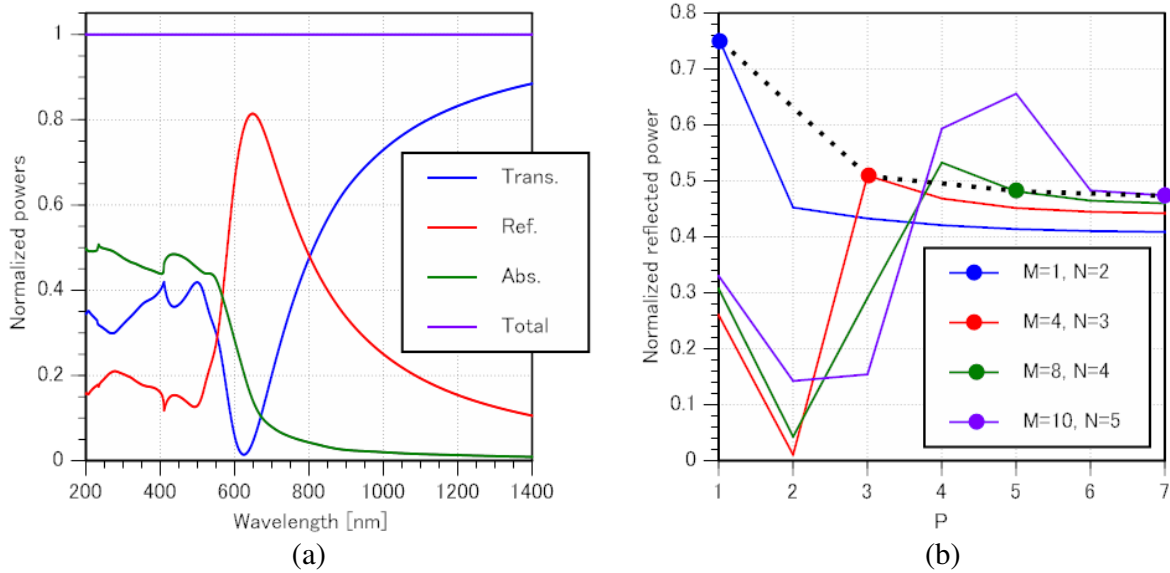

Figure 5. Normalized powers for a disk array, the parameters of which are the same as those in Fig. 2(a). (a) Power distribution at $P = 5$, $M = 8$, and $N = 4$. (b) Reflected power at $\lambda = 800\,\text{nm}$.

where, in terms of the symbol $\rho = 2\pi a/d$, the normalized admittances are expressed as

$$
\left.
\begin{aligned}
\frac{1}{\bar{Y}^J} &= \frac{4\pi\left(\xi_{11}'^2 - 1\right)}{\rho^2}\frac{R}{\zeta_0} - j8\left\{\sqrt{\left(\frac{\lambda}{d}\right)^2 - 1}\left[\frac{J_1(\rho)}{\rho}\right]^2 - \frac{1}{\sqrt{(\lambda/d)^2 - 1}}\left[\frac{J_1'(\rho)}{1 - (\rho/\xi_{11}')^2}\right]^2\right. \\
&\quad \left. + \sqrt{2\left(\frac{\lambda}{d}\right)^2 - 1}\left[\frac{J_1\left(\sqrt{2}\rho\right)}{\sqrt{2}\rho}\right]^2 - \frac{1}{\sqrt{2(\lambda/d)^2 - 1}}\left[\frac{J_1'\left(\sqrt{2}\rho\right)}{1 - \left(\sqrt{2}\rho/\xi_{11}'\right)^2}\right]^2\right\}
\end{aligned}
\right\} \text{ (disks) (31)}
$$

$$
\bar{Y}^M = 1/\bar{Y}^J\big|_{R/\zeta_0 \to Q\zeta_0}
$$

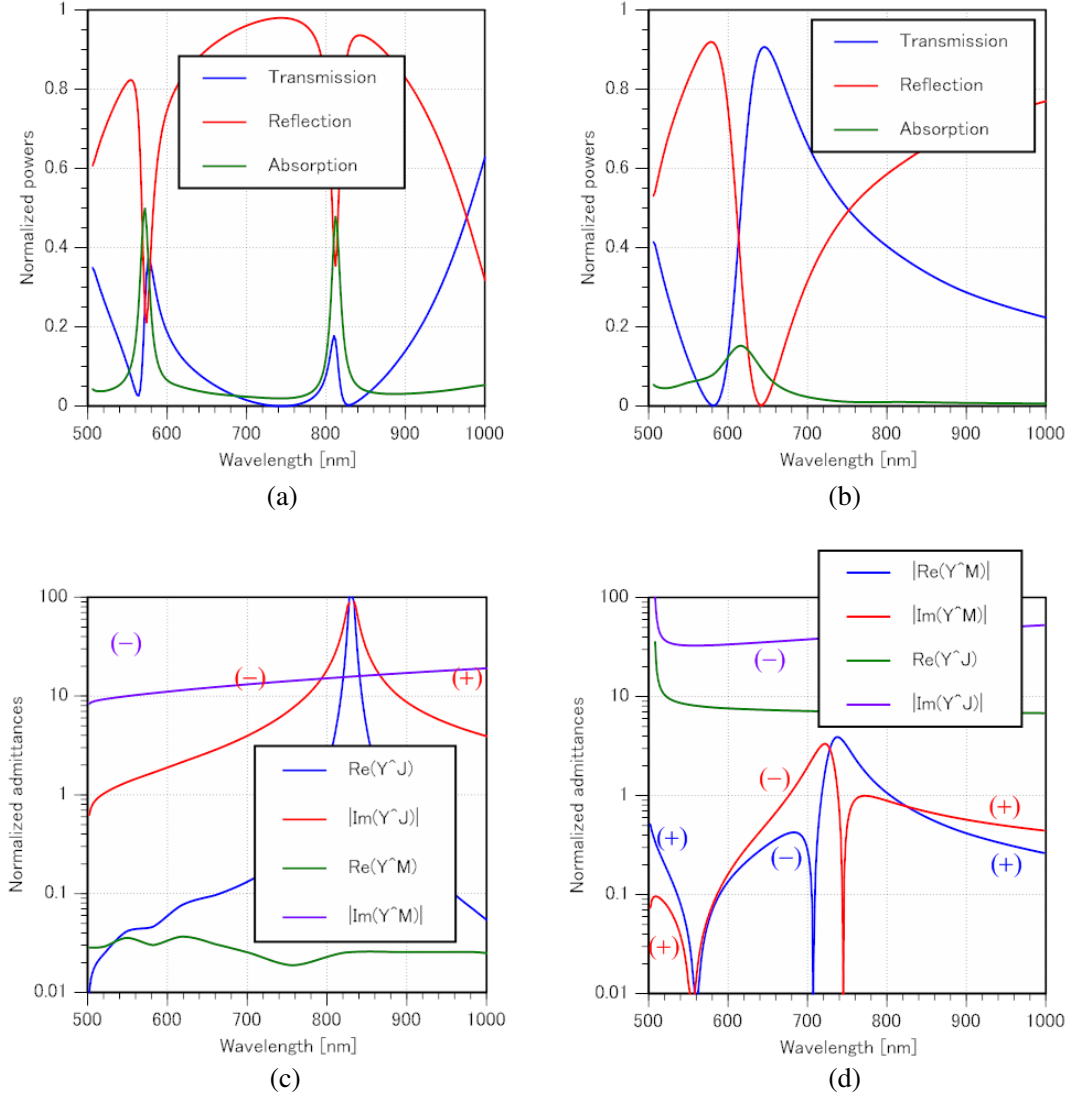**Figure 6.** Normalized powers and admittances for silver arrays in the single mode range at normal incidence. The size is given by $d = 500\,\text{nm}$, $b = 30\,\text{nm}$, and $a = 250\,\text{nm}$ (for disks), and $131\,\text{nm}$ (for apertures). (a) Powers for disks. (b) Powers for apertures. (c) Admittances for disks. (d) Admittances for apertures.

$$\frac{1}{\bar{Y}^M} = \frac{2R}{\zeta_0} - j8\left(1 + \frac{2R}{\zeta_0}\right)^2 \left\{ \frac{\left[\frac{J_1'(\rho)}{1-(\rho/\xi_{11}')^2}\right]^2}{\frac{1}{\sqrt{(\lambda/d)^2-1}} - \frac{j2R}{\zeta_0}} - \frac{\left[\frac{J_1(\rho)}{\rho}\right]^2}{\sqrt{\left(\frac{\lambda}{d}\right)^2-1} + \frac{j2R}{\zeta_0}} \right.$$

$$\left. + \frac{\left[\frac{J_1'\left(\sqrt{2}\rho\right)}{1-\left(\sqrt{2}\rho/\xi_{11}'\right)^2}\right]^2}{\frac{1}{\sqrt{2(\lambda/d)^2-1}} - \frac{j2R}{\zeta_0}} - \frac{\left[\frac{J_1\left(\sqrt{2}\rho\right)}{\sqrt{2}\rho}\right]^2}{\sqrt{2\left(\frac{\lambda}{d}\right)^2-1} + \frac{j2R}{\zeta_0}} \right\} \quad \text{(apertures)} \quad (32)$$

$$\bar{Y}^J = 1/\bar{Y}^M\big|_{R/\zeta_0 \to Q\zeta_0}$$

Note that $1/\bar{Y}^M$ in (32) along with $R = 0$ is reduced to Eq. (11) of [14] for the PEC case.

Figures 6(a), (b) show the transmitted, reflected, and absorbed powers normalized by the incident one for the arrays of disks and apertures in the single mode range. In the disk case (a), the radius is taken the largest as it can be, so that the adjacent disks just contact with each other. The area of the disk for (a) is $0.196\,\mu\text{m}^2$, which is the same as that of the metal part included in the unit cell for (b). Variations of the powers in (a) and (b) are explained by the behavior of normalized admittances plotted in (c) and (d), respectively. The discussions are as follows.

- The admittances $\bar{Y}^J$ in (31) and $\bar{Y}^M$ in (32) are both purely imaginary for PEC because of $R = 0$. The introduction of R for noble metals makes the admittances complex. Its imaginary (real) part affect the variation of the transmitted and reflected powers (absorbed power).

- The admittances $\bar{Y}^M$ in (31) and $\bar{Y}^J$ in (32) are both infinity for PEC since $|Q| \to \infty$. This is related to the fact that there is no flow of magnetic (electric) current on the disks (apertures). The finiteness of these admittances in noble metals gives an odd contribution toward transmitted and reflected sides through (30).

- In the disk case (a), rapid change in powers occurs when the circumference of the disk, $1570\,\text{nm}$, is approximately integral times as wavelength. This is related with the multipole resonance.

6. CONCLUSION

Numerical solution has been developed to investigate the power distributions of two-dimensional periodic arrays of disks and circular apertures with regard to thin noble-metals. Enforcing the generalized boundary conditions leads us to the set of integral equations, which is treated by means of the method of moments. The computations are carried out to find power distributions as a function of wavelength and array parameters. The results are discussed in terms of Rayleigh wavelength, and partly, treated in the context of extraordinary transmission with the aid of quasi-static solutions.

Though interesting results have been obtained, the present work has limited to treating free-standing structures and showing transmitted and reflected powers which are related with far field. Now it will become important to introduce semi-infinite or layered dielectric substrate in order to model practical structure such as sensors, solar cells, plasmonic lenses, and so on. In this case, we need to compute the distribution of near evanescent field to demonstrate the enhancement of electric field density. When treating plates or holes with general shapes, basis functions are obtained by solving eigenvalue problem of Helmholtz's equation by means of the finite element method [25]. Furthermore, it is important to clarify the validity of the generalized boundary conditions by comparing with the exact solution, especially when the surface waves are excited and the fields are localized. These problems deserve further attention.

APPENDIX A. EXACT COEFFICIENTS FOR AN INFINITE SHEET

When we exactly apply the boundary conditions on the surfaces of an infinite sheet, $y = \pm b/2$, the coefficients of the transmitted and reflected plane waves are obtained as

$$\begin{pmatrix} A_s \\ B_s \end{pmatrix} = \left(-\frac{1 - 2R_s\eta_{s00}}{1 + 2R_s\eta_{s00}} \mp \frac{1 - 2Q_s/\eta_{s00}}{1 + 2Q_s/\eta_{s00}} \right) \frac{V_s}{2} e^{jk_0 b\cos\theta^i} \quad (s = 1 : \text{TE}, \ s = 2 : \text{TM}) \qquad (\text{A1})$$

where

$$\begin{pmatrix} R_1/\zeta_0 \\ R_2/\zeta_0 \\ Q_1\zeta_0 \\ Q_2\zeta_0 \end{pmatrix} = \begin{pmatrix} 1/\sqrt{\tilde{\varepsilon}_r} \\ \sqrt{\tilde{\varepsilon}_r}/\varepsilon_r \\ \sqrt{\tilde{\varepsilon}_r} \\ \varepsilon_r/\sqrt{\tilde{\varepsilon}_r} \end{pmatrix} \frac{1}{2j} \cot \frac{k_0 b\sqrt{\tilde{\varepsilon}_r}}{2}, \quad \tilde{\varepsilon}_r = \varepsilon_r - \sin^2\theta^i \qquad (\text{A2})$$

From the material condition $|\varepsilon_r| \gg 1$ we can say that $\sqrt{\tilde{\varepsilon}_r} \approx \sqrt{\varepsilon_r}$, and thereby (A2) approaches (4). Further the size condition $b \ll \lambda$ leads to $e^{jk_0 b \cos \theta^i} \approx 1$, from which (A1) is reduced to (11).

APPENDIX B. INNER PRODUCTS

The inner products (24) defined by the double integrals are analytically evaluated as follows.

$$\begin{cases} C_{1mn,1pq} = -\dfrac{2\sqrt{\pi} m j^m e^{jm\phi_{pq}}}{\sqrt{\xi_{mn}'^2 - m^2}\sqrt{\alpha_p^2 + \beta_q^2} d} J_m \left(\sqrt{\alpha_p^2 + \beta_q^2}\, a \right) \\[4mm] C_{1mn,2pq} = \dfrac{a}{d} \dfrac{2\sqrt{\pi} j^{m-1} \xi_{mn}'^2 e^{jm\phi_{pq}}}{\sqrt{\xi_{mn}'^2 - m^2}\left[\xi_{mn}'^2 - (\alpha_p^2 + \beta_q^2)a^2\right]} J_m' \left(\sqrt{\alpha_p^2 + \beta_q^2}\, a \right) \\[4mm] C_{2mn,1pq} = \dfrac{a}{d} \dfrac{2\sqrt{\pi} j^{m-1} e^{jm\phi_{pq}} \sqrt{\alpha_p^2 + \beta_q^2}\, a}{\xi_{mn}^2 - (\alpha_p^2 + \beta_q^2)a^2} J_m \left(\sqrt{\alpha_p^2 + \beta_q^2}\, a \right) \\[4mm] C_{2mn,2pq} = 0 \end{cases} \tag{B1}$$

where $e^{j\phi_{pq}} = (\alpha_p + j\beta_q)/\sqrt{\alpha_p^2 + \beta_q^2}$. In carrying out the integrals with respect to ϕ and r, we made use of the integral representation of the Bessel function and the differentiation formulas

$$\begin{cases} \dfrac{d}{dr}\left[J_m(\alpha r)J_m(\beta r)\right] = \alpha J_m'(\alpha r)J_m(\beta r) + \beta J_m(\alpha r)J_m'(\beta r) \\[3mm] \dfrac{d}{dr}\left[\alpha r J_m(\alpha r)J_m'(\beta r) - \beta r J_m'(\alpha r)J_m(\beta r)\right] = (\alpha^2 - \beta^2)\left[r J_m'(\alpha r)J_m'(\beta r) + \dfrac{m^2}{\alpha\beta r}J_m(\alpha r)J_m(\beta r)\right] \end{cases} \tag{B2}$$

respectively. Here, the prime denotes differentiation with respect to the argument.

REFERENCES

1. Maier, S. A., *Plasmonics: Fundamentals and Applications*, Springer, 2007.
2. Kim, K. Y., *Plasmonics: Principles and Applications*, InTech, 2012.
3. Natarov, D. M., V. O. Byelobrov, R. Sauleau, T. M. Benson, and A. I. Nosich, "Periodicity-induced effects in the scattering and absorption of light by infinite and finite gratings of circular silver nanowires," *Optics Express*, Vol. 19, No. 22, 22176–22190, 2011.
4. Shapoval, O. V., R. Sauleau, and A. I. Nosich, "Modeling of plasmon resonances of multiple flat noble-metal nanostrips with a median-line integral equation technique," *IEEE Trans. Nanotechnology*, Vol. 12, No. 3, 442–449, 2013.
5. Shapoval, O. V., A. I. Nosich, and J. Čtyroký, "Resonance effects in the optical antennas shaped as finite comb-like gratings of noble-metal nanostrips," *SPIE Proc. 8781 (Integrated Optics: Physics and Simulations)*, No. 87810U, 1–8, 2013.
6. Ebbesen, T. W., H. J. Lezec, H. F. Ghaemi, T. Thio, and P. A. Wolff, "Extraordinary optical transmission through sub-wavelength hole arrays," *Nature*, Vol. 391, 667–669, 1998.
7. Glushko, O., R. Brunner, R. Meisels, S. Kalchmair, and G. Strasser, "Extraordinary transmission in metal hole array-photonic crystal hybrid structures," *Optics Express*, Vol. 20, No. 15, 17174–17182, 2012.
8. Bleszynski, E., M. Bleszynski, and T. Jaroszewicz, "Surface-integral equations for electromagnetic scattering from impenetrable and penetrable sheets," *IEEE Antennas Propag. Mag.*, Vol. 35, No. 6, 14–25, 1993.
9. Senior, T. B. A. and J. L. Volakis, *Approximate Boundary Conditions in Electromagnetics*, IEE, London, 1995.
10. Shapoval, O. V., R. Sauleau, and A. I. Nosich, "Scattering and absorption of waves by flat material strips analyzed using generalized boundary conditions and Nystrom-type algorithm," *IEEE Trans. Antennas Propagat.*, Vol. 59, No. 9, 3339–3346, 2011.
11. Munk, B. A., *Frequency Selective Surfaces: Theory and Design*, John Wiley & Sons, 2000.

12. Amitay, N. and V. Galindo, "The analysis of circular waveguide phased arrays," *Bell Syst. Tech. J.*, Vol. 47, No. 9, 1903–1932, 1968.

13. Chen, C. C., "Diffraction of electromagnetic waves by a conducting screen perforated periodically with circular holes," *IEEE Trans. Microwave Theory Tech.*, Vol. 19, No. 5, 475–481, 1971.

14. Chen, C. C., "Transmission of microwave through perforated flat plates of finite thickness," *IEEE Trans. Microwave Theory Tech.*, Vol. 21, No. 1, 1–6, 1973.

15. Koledintseva, M. Y., J. Huang, J. L. Drewniak, R. E. DuBroff, and B. Archambeault, "Modeling of metasheets embedded in dielectric layers," *Progress In Electromagnetics Research B*, Vol. 44, 89–116, 2012.

16. Hamdi, B., T. Aguili, and H. Baudrand, "Floquet modal analysis to modelize and study 2-D planar almost periodic structures in finite and infinite extent with coupled motifs," *Progress In Electromagnetics Research B*, Vol. 62, 63–86, 2015.

17. Matsushima, A., T. L. Zinenko, H. Nishimori, and Y. Okuno, "Plane wave scattering from perpendicularly crossed multilayered strip gratings," *Progress In Electromagnetics Research*, Vol. 28, 185–203, 2000.

18. Matsushima, A., Y. Momoka, M. Ohtsu, and Y. Okuno, "Efficient numerical approach to electromagnetic scattering from three-dimensional periodic array of dielectric spheres using sequential accumulation," *Progress In Electromagnetics Research*, Vol. 69, 305–322, 2007.

19. Harrington, R. F., *Field Computation by Moment Methods*, Macmillan, New York, 1968.

20. Braver, I. M., P. Sh. Fridberg, K. L. Garb, and I. M. Yakover, "The behavior of the electromagnetic field near the edge of a resistive half-plane," *IEEE Trans. Antennas Propagat.*, Vol. 36, No. 12, 1760–1768, 1988.

21. Mittra, R., T. Itoh, and T. S. Li, "Analytical and numerical studies of the relative convergence phenomenon arising in the solution of an integral equation by the moment method," *IEEE Trans. Microwave Theory Tech.*, Vol. 20, No. 2, 96–104, 1972.

22. Johnson, P. B. and R. W. Christy, "Optical constants of the noble metals," *Phys. Rev.*, Vol. 6, 4370–4379, 1972.

23. Amitay, N. and V. Galindo, "On energy conservation and the method of moments in scattering problems," *IEEE Trans. Antennas Propagat.*, Vol. 17, No. 7, 747–751, 1969.

24. Lee, S. W., G. Zarrillo, and C. L. Law, "Simple formulas for transmission through periodic metal grids or plates," *IEEE Trans. Antennas Propagat.*, Vol. 30, No. 5, 904–909, 1982.

25. Widenberg, B., S. Poulsen, and A. Karlsson, "Scattering from thick frequency selective screens," *Journal of Electromagnetic Waves and Applications*, Vol. 14, No. 9, 1303–1328, 2000.